Electronic Supplementary Information

How End-Capped Acceptors Regulate the Photovoltaic Performance of the Organic Solar Cells: A Detailed Density Functional Exploration of Their Impact on the A-D-π-D-A Type Small Molecular Electron Donors

*Paramasivam Mahalingavelar**

Center for Optoelectronic Materials and Devices, School of Polymer Science and Engineering, The University of Southern Mississippi, Hattiesburg, Mississippi 39406, United States.

Table of contents

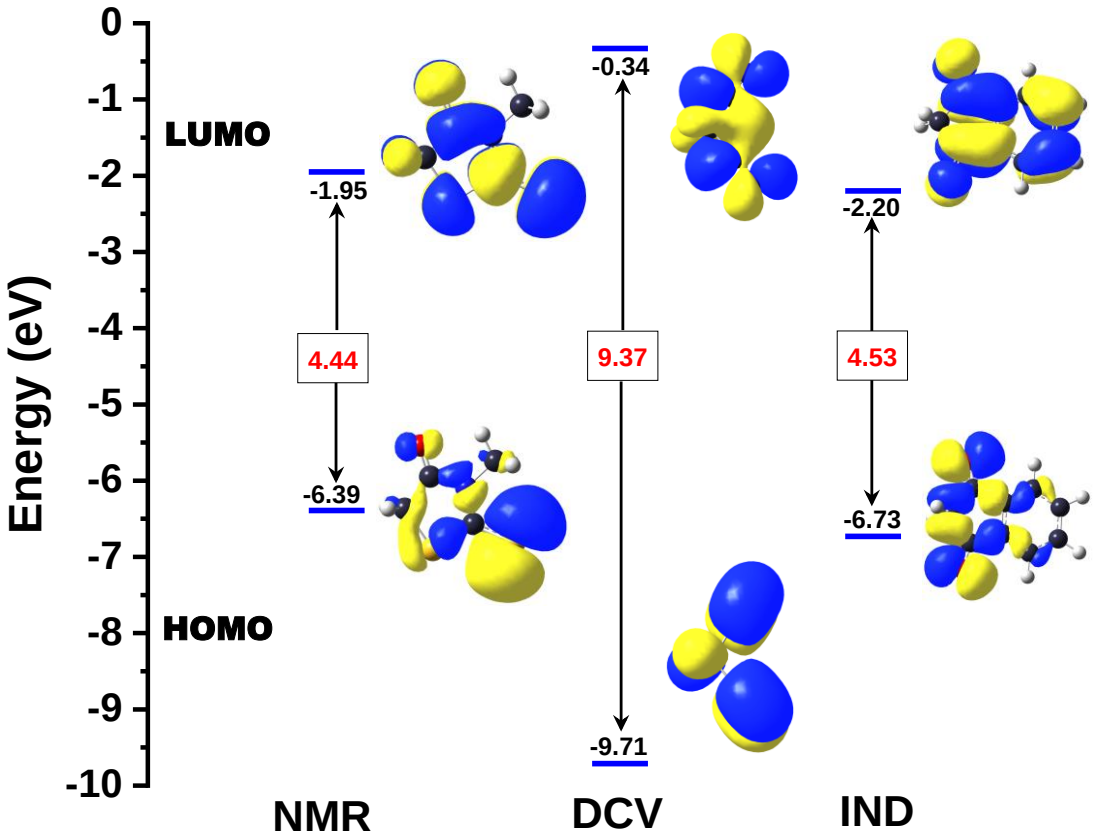

Figure S1. DFT computed HOMO, LUMO, HOMO-LUMO gap and isodensity plots of the bare acceptors obtained at the DFT/B3LYP/6-311G(d, p) level of theory.

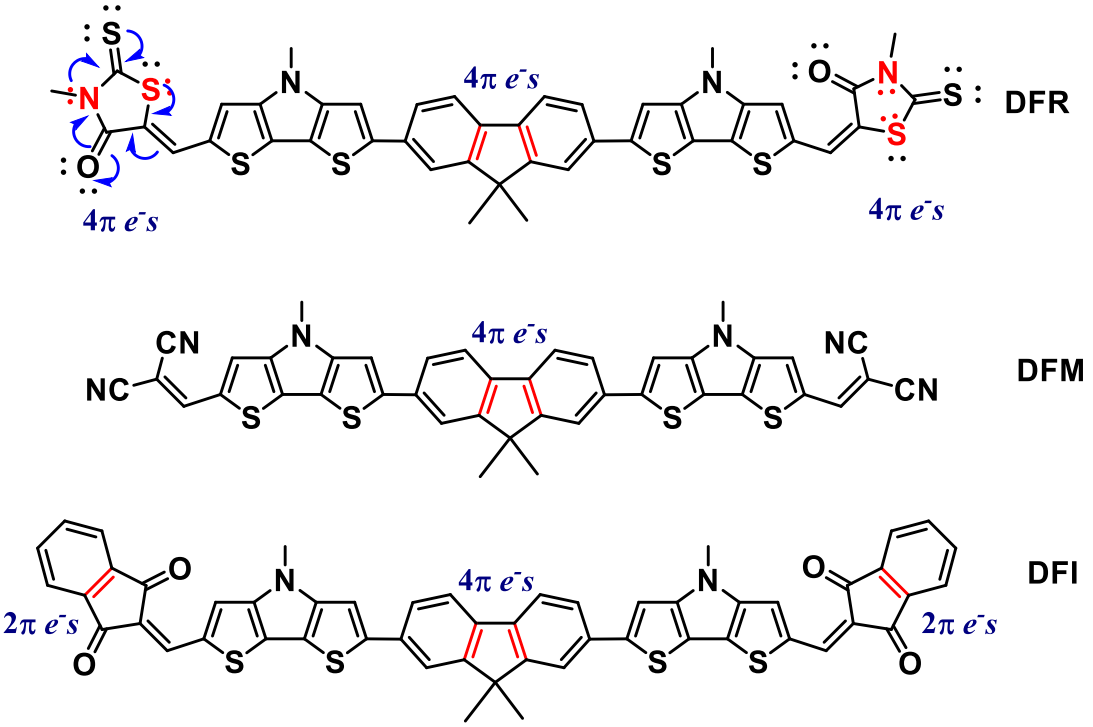

Figure S2. Existence of anti-aromatic units in the SMEDs. (Indicated red in color)

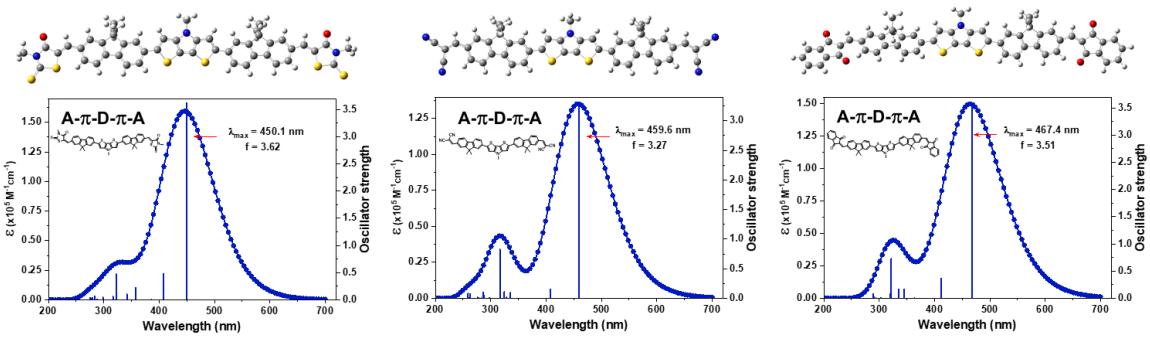

Figure S3. Optimized geometries, simulated absorptions and oscillator strength of the A-π-D-π-A framework using DFT/B3LYP/6-311G(d, p)/CPCM(CH_2Cl_2)//TDDFT/M062X/6-311G(d, p)/CPCM (CH_2Cl_2) level of theory.

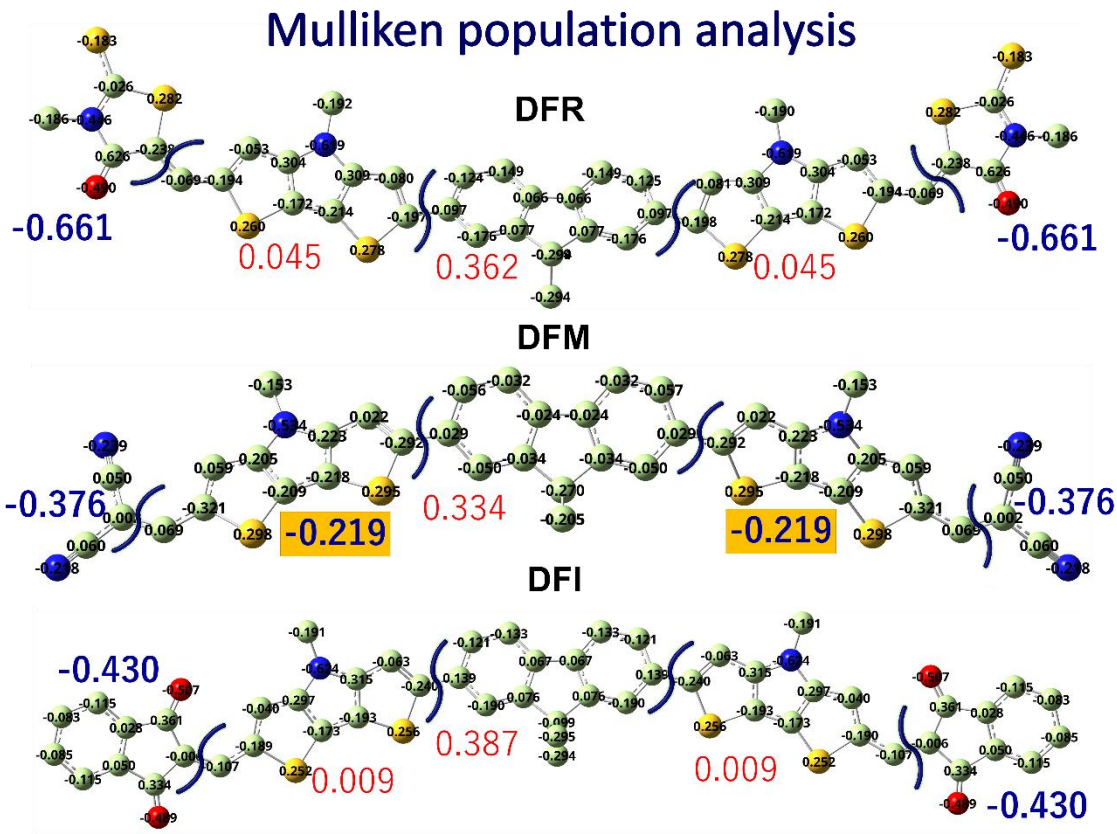

Figure S4. Mulliken population analysis on the grouped segments (D, π and A) of the SMEDs obtained from DFT/B3LYP/6-311++G (d, p) level of theory.

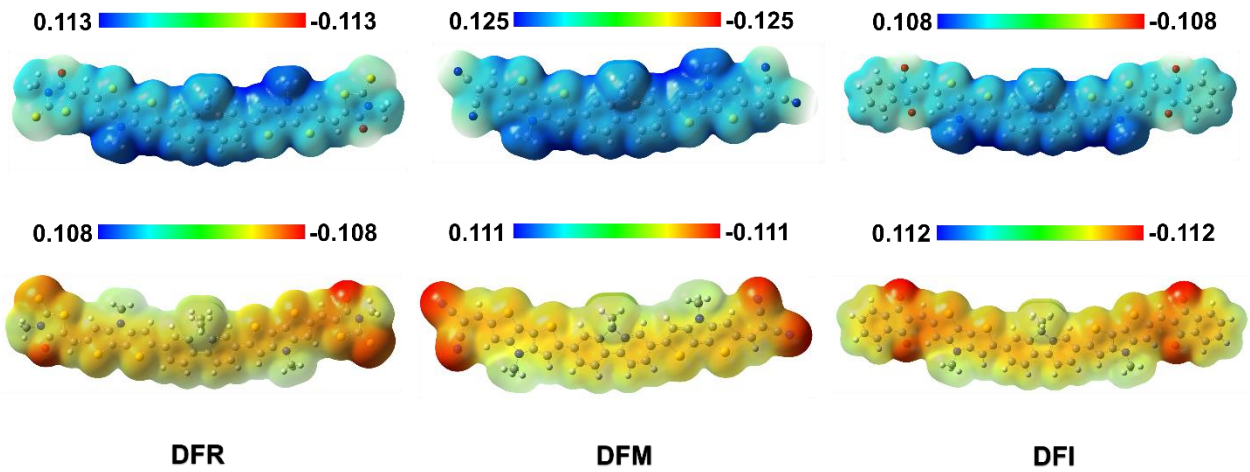

Figure S5. Variation of electrostatic environment revealed from MESP plots of the SMEDs at the oxidized (*-1e*$^-$) and reduced (*+1e*$^-$) states.

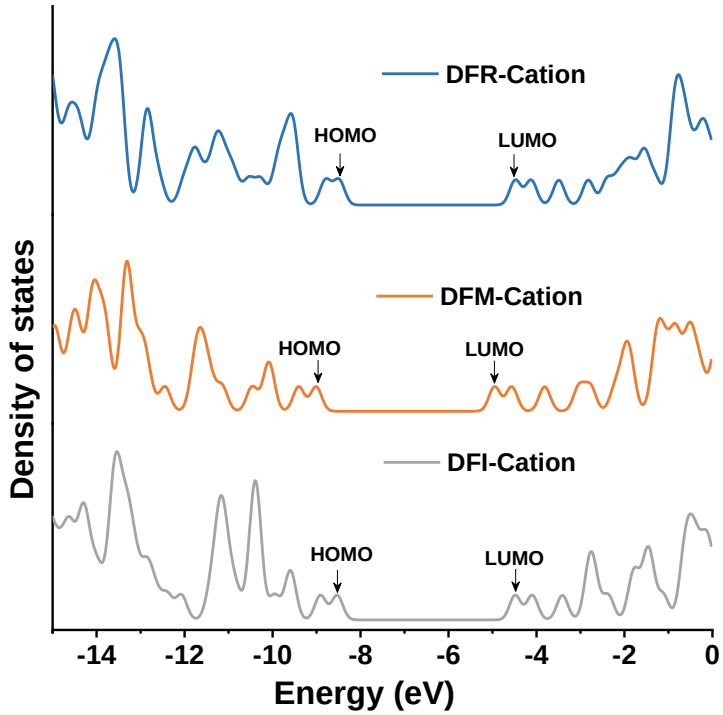

Figure S6 Variation of energy levels in terms of DOS population corresponding to the HOMO and LUMO of the SMEDs at the oxidized (*-1e*$^-$) state.

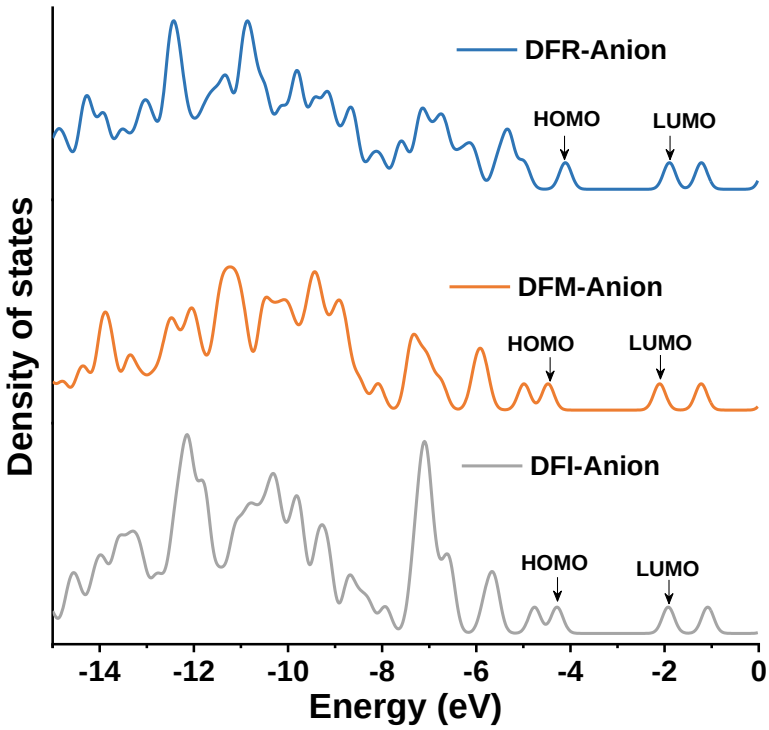

Figure S7. Variation of energy levels in terms of DOS population corresponding to the HOMO and LUMO of the SMEDs at the reduced (*+1e*$^-$) state.

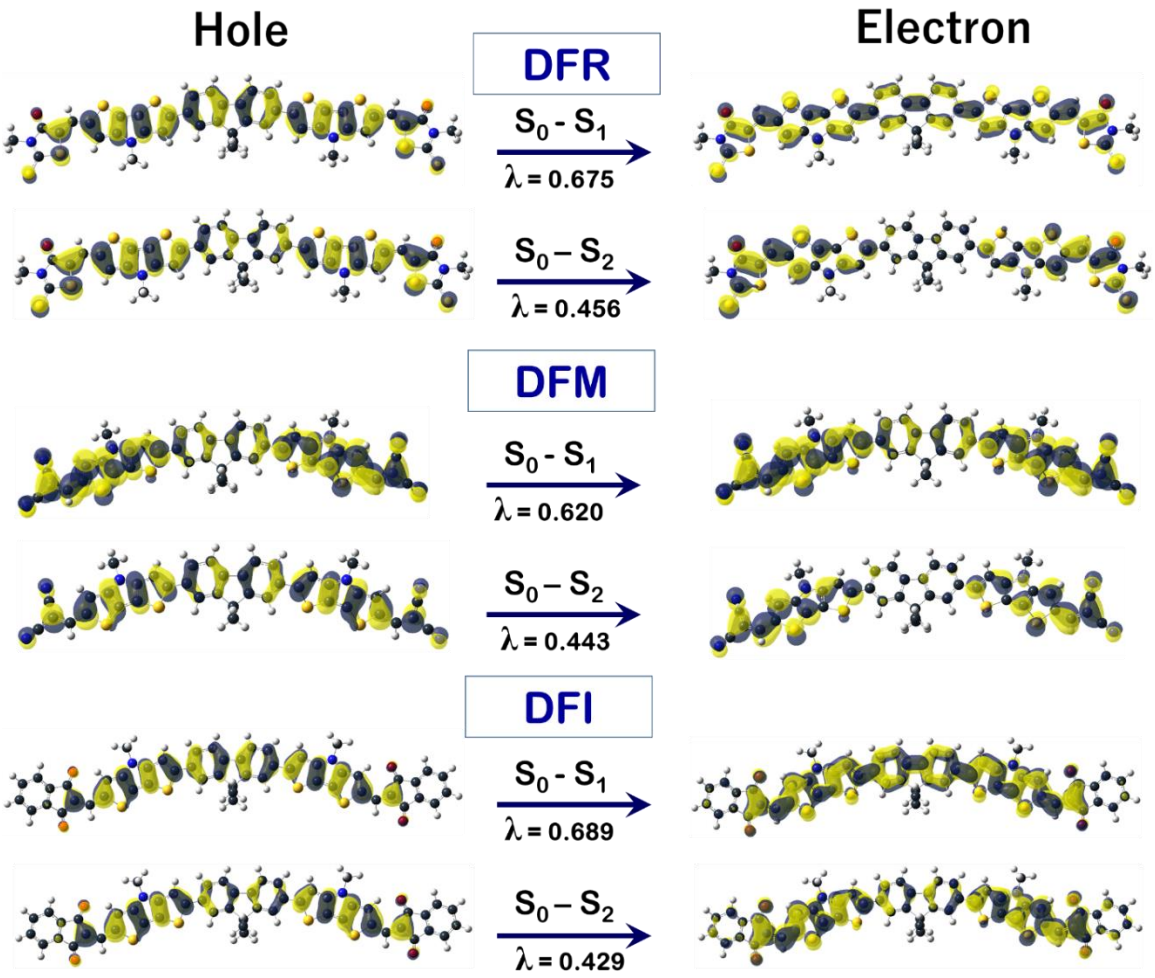

Figure S8. Natural transition orbital (NTOs) analysis corresponding to S_0-S_1 and S_0-S_2 transitions.

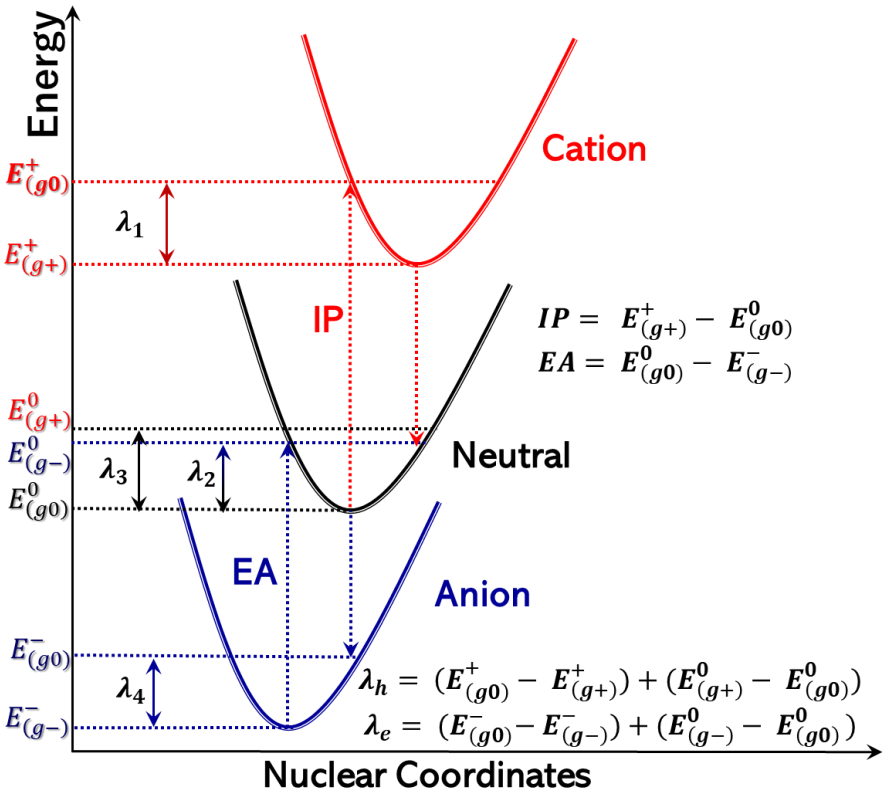

Figure S9. Schematic diagram represents the computational methodology for reorganization energy calculations.

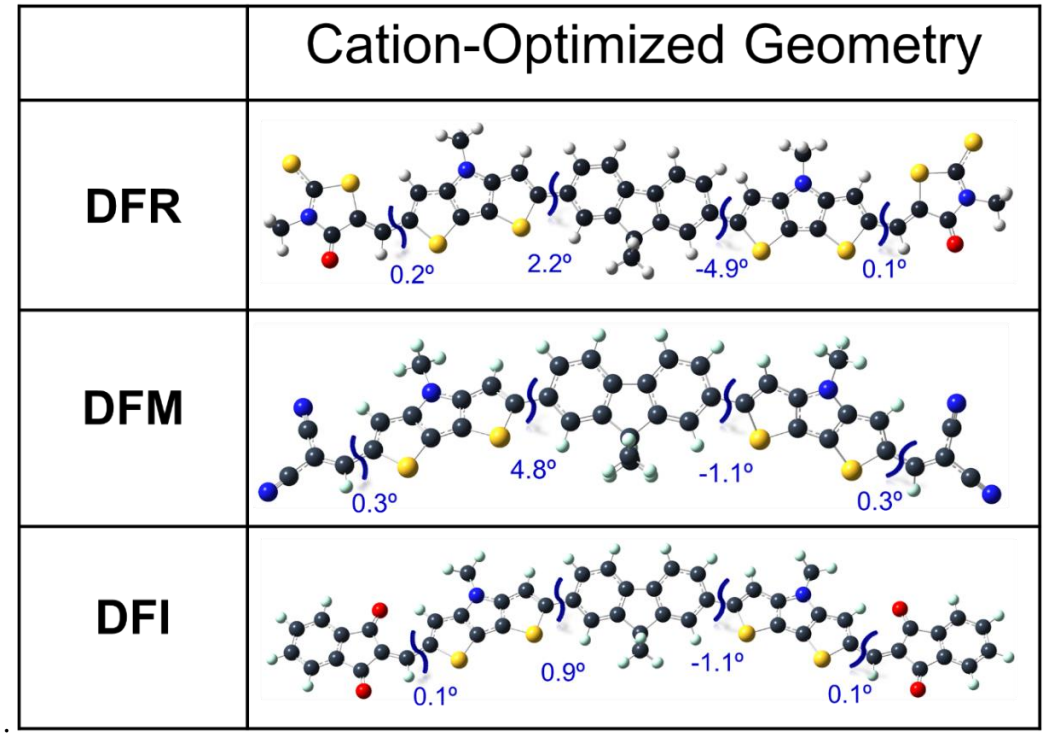

Figure S10. Optimized geometry of SMEDs with selected dihedral angles in their first oxidized (cationic) state.

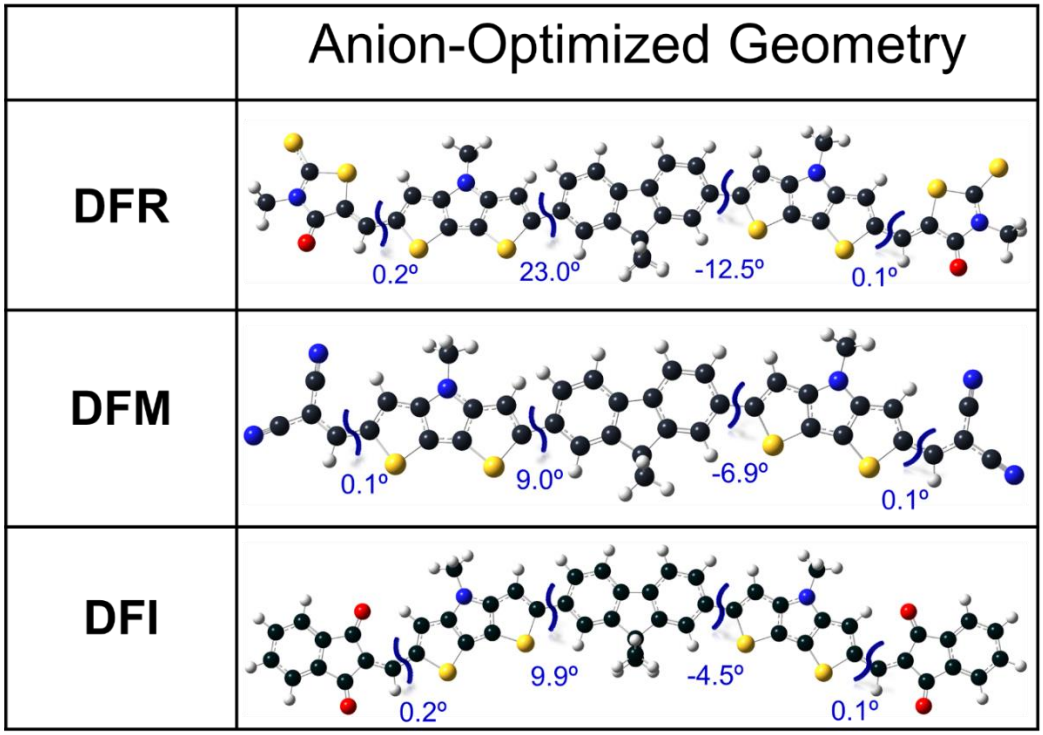

Figure S11. Optimized geometry of SMEDs with selected dihedral angles in their first reduced (anionic) state.

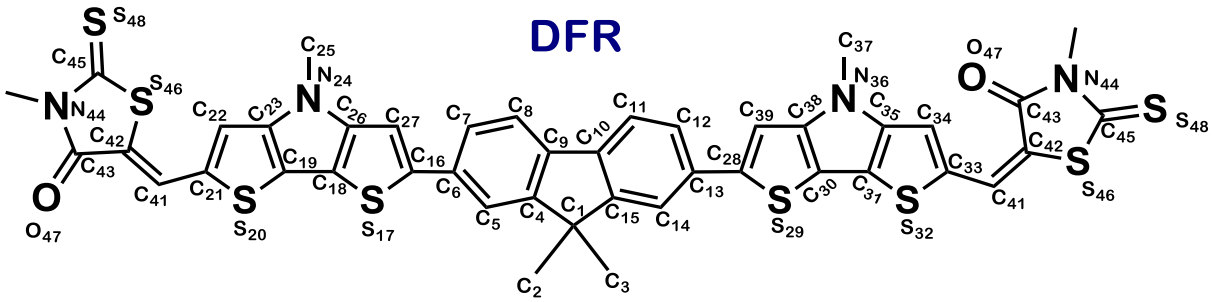

DFR	Neutral	Cation	Anion		DFR	Neutral	Cation	Anion
C_1-C_2	1.544	1.541	1.545		C_{26}-C_{27}	1.414	1.397	1.404
C_1-C_3	1.544	1.541	1.545		C_{27}-C_{16}	1.379	1.394	1.388
C_1-C_4	1.529	1.527	1.529		C_{13}-C_{28}	1.463	1.440	1.459
C_4-C_5	1.383	1.376	1.382		C_{28}-S_{29}	1.774	1.784	1.781
C_5-C_6	1.411	1.418	1.416		S_{29}-C_{30}	1.729	1.733	1.740
C_6-C_7	1.408	1.422	1.417		C_{30}-C_{31}	1.406	1.392	1.401
C_7-C_8	1.389	1.379	1.386		C_{31}-S_{32}	1.729	1.731	1.730
C_8-C_9	1.395	1.405	1.400		S_{32}-C_{33}	1.782	1.781	1.788
C_4-C_9	1.408	1.417	1.409		C_{33}-C_{34}	1.391	1.395	1.396
C_9-C_{10}	1.461	1.441	1.456		C_{34}-C_{35}	1.402	1.397	1.398
C_{10}-C_{11}	1.395	1.404	1.398		C_{35}-N_{36}	1.385	1.380	1.383
C_{11}-C_{12}	1.388	1.380	1.389		N_{36}-C_{37}	1.451	1.459	1.455
C_{12}-C_{13}	1.408	1.418	1.410		N_{36}-C_{38}	1.382	1.378	1.393
C_{13}-C_{14}	1.411	1.420	1.414		C_{38}-C_{39}	1.414	1.397	1.412
C_{14}-C_{15}	1.383	1.375	1.381		C_{39}-C_{28}	1.462	1.394	1.381
C_{15}-C_{10}	1.408	1.417	1.412		C_{21}-C_{41}	1.423	1.422	1.415
C_{15}-C_1	1.529	1.528	1.529		C_{41}-C_{42}	1.359	1.361	1.367
C_6-C_{16}	1.463	1.442	1.451		C_{33}-C_{41}	1.421	1.422	1.419
C_{16}-S_{17}	1.774	1.783	1.789		C_{42}-C_{43}	1.415	1.420	1.420
S_{17}-C_{18}	1.737	1.734	1.741		C_{43}-N_{44}	1.473	1.462	1.462
C_{18}-C_{19}	1.406	1.392	1.348		N_{44}-C_{45}	1.368	1.359	1.359
C_{19}-S_{20}	1.729	1.731	1.743		C_{45}-S_{46}	1.777	1.756	1.766
S_{20}-C_{21}	1.782	1.781	1.806		C_{42}-S_{46}	1.648	1.653	1.663
C_{21}-C_{22}	1.391	1.395	1.400		C_{43}-O_{47}	1.213	1.213	1.219
C_{22}-C_{23}	1.402	1.398	1.408					
C_{23}-N_{24}	1.385	1.379	1.384					
N_{24}-C_{25}	1.451	1.459	1.453					
N_{24}-C_{26}	1.382	1.379	1.386					

Figure S12. Optimized geometrical coordinates of DFR at the neutral, cation and anionic states.

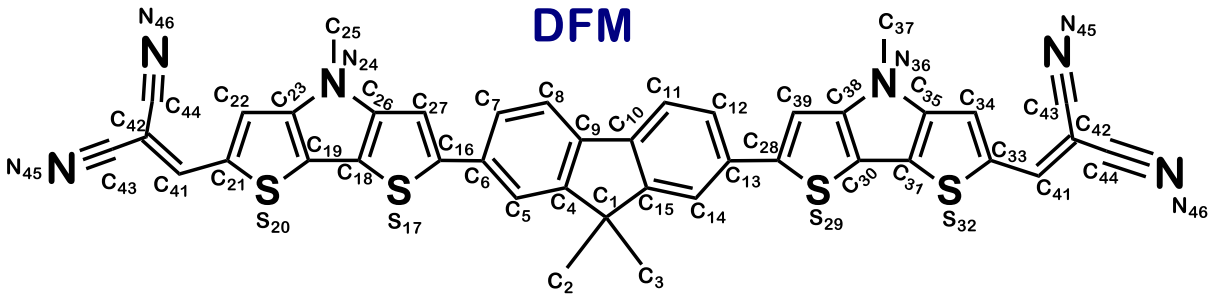

DFM	Neutral	Cation	Anion		DFM	Neutral	Cation	Anion
C_1-C_2	1.544	1.545	1.544		N_{24}-C_{25}	1.453	1.459	1.455
C_1-C_3	1.544	1.545	1.544		N_{24}-C_{26}	1.380	1.377	1.381
C_1-C_4	1.528	1.527	1.530		C_{26}-C_{27}	1.413	1.397	1.404
C_4-C_5	1.383	1.380	1.378		C_{27}-C_{16}	1.379	1.395	1.388
C_5-C_6	1.409	1.421	1.419		C_{13}-C_{28}	1.463	1.440	1.448
C_6-C_7	1.409	1.423	1.415		C_{28}-S_{29}	1.774	1.783	1.788
C_7-C_8	1.388	1.378	1.386		S_{29}-C_{30}	1.726	1.732	1.741
C_8-C_9	1.396	1.406	1.400		C_{30}-C_{31}	1.403	1.392	1.393
C_4-C_9	1.407	1.418	1.414		C_{31}-S_{32}	1.726	1.726	1.735
C_9-C_{10}	1.460	1.438	1.450		S_{32}-C_{33}	1.786	1.782	1.804
C_{10}-C_{11}	1.396	1.405	1.402		C_{33}-C_{34}	1.395	1.398	1.411
C_{11}-C_{12}	1.388	1.378	1.384		C_{34}-C_{35}	1.396	1.393	1.390
C_{12}-C_{13}	1.409	1.421	1.418		C_{35}-N_{36}	1.385	1.380	1.385
C_{13}-C_{14}	1.409	1.421	1.417		N_{36}-C_{37}	1.453	1.459	1.454
C_{14}-C_{15}	1.383	1.374	1.380		N_{36}-C_{38}	1.380	1.376	1.382
C_{15}-C_{10}	1.407	1.419	1.412		C_{38}-C_{39}	1.413	1.397	1.403
C_{15}-C_1	1.528	1.527	1.530		C_{38}-C_{28}	1.463	1.394	1.390
C_6-C_{16}	1.463	1.441	1.448		C_{21}-C_{41}	1.418	1.419	1.404
C_{16}-S_{17}	1.774	1.782	1.787		C_{41}-C_{42}	1.379	1.376	1.395
S_{17}-C_{18}	1.738	1.732	1.741		C_{33}-C_{41}	1.422	1.419	1.398
C_{18}-C_{19}	1.402	1.392	1.394		C_{42}-C_{43}	1.425	1.425	1.412
C_{19}-S_{20}	1.726	1.726	1.733		C_{42}-C_{44}	1.422	1.422	1.415
S_{20}-C_{21}	1.786	1.782	1.801		C_{43}-N_{45}	1.186	1.156	1.161
C_{21}-C_{22}	1.395	1.398	1.409		C_{44}-N_{46}	1.187	1.157	1.161
C_{22}-C_{23}	1.396	1.394	1.390					
C_{23}-N_{24}	1.385	1.380	1.384					

Figure S13. Optimized geometrical coordinates of DFM at the neutral, cation and anionic states.

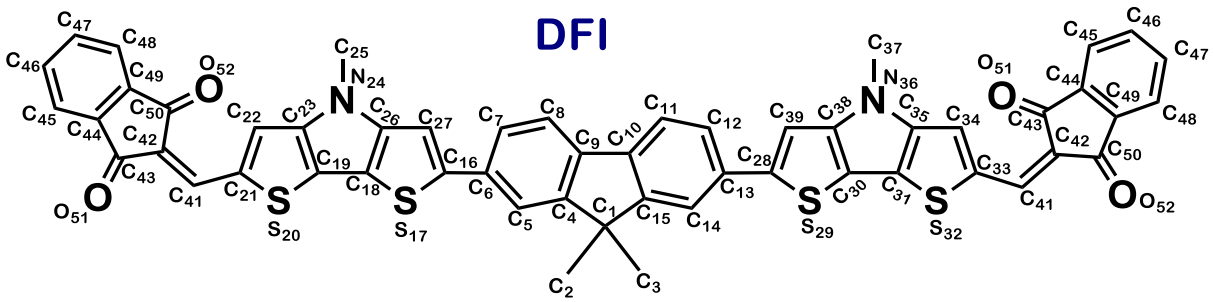

DFI	Neutral	Cation	Anion		DFI	Neutral	Cation	Anion
C_1-C_2	1.544	1.545	1.541		C_{30}-C_{31}	1.404	1.391	1.392
C_1-C_3	1.544	1.545	1.541		C_{31}-S_{32}	1.726	1.729	1.735
C_1-C_4	1.528	1.527	1.526		S_{32}-C_{33}	1.790	1.786	1.801
C_4-C_5	1.383	1.375	1.379		C_{33}-C_{34}	1.394	1.396	1.410
C_5-C_6	1.409	1.419	1.418		C_{34}-C_{35}	1.396	1.395	1.391
C_6-C_7	1.409	1.422	1.417		C_{35}-N_{36}	1.387	1.381	1.387
C_7-C_8	1.388	1.378	1.387		N_{36}-C_{37}	1.452	1.459	1.454
C_8-C_9	1.396	1.405	1.401		N_{36}-C_{38}	1.379	1.377	1.381
C_4-C_9	1.407	1.417	1.412		C_{38}-C_{39}	1.414	1.397	1.405
C_9-C_{10}	1.461	1.440	1.450		C_{38}-C_{28}	1.461	1.395	1.391
C_{10}-C_{11}	1.396	1.405	1.401		C_{21}-C_{41}	1.416	1.421	1.419
C_{11}-C_{12}	1.388	1.378	1.387		C_{41}-C_{42}	1.369	1.366	1.396
C_{12}-C_{13}	1.409	1.422	1.418		C_{33}-C_{41}	1.420	1.421	1.411
C_{13}-C_{14}	1.409	1.419	1.418		C_{42}-C_{43}	1.476	1.482	1.456
C_{14}-C_{15}	1.383	1.375	1.378		C_{43}-C_{44}	1.395	1.493	1.508
C_{15}-C_{10}	1.406	1.417	1.379		C_{44}-C_{45}	1.386	1.390	1.384
C_{15}-C_1	1.528	1.527	1.526		C_{45}-C_{46}	1.395	1.395	1.403
C_6-C_{16}	1.462	1.442	1.450		C_{46}-C_{47}	1.401	1.402	1.394
C_{16}-S_{17}	1.774	1.783	1.789		C_{47}-C_{48}	1.395	1.395	1.403
S_{17}-C_{18}	1.738	1.733	1.741		C_{48}-C_{49}	1.395	1.390	1.385
C_{18}-C_{19}	1.404	1.391	1.393		C_{49}-C_{50}	1.398	1.489	1.499
C_{19}-S_{20}	1.726	1.729	1.734		C_{42}-C_{50}	1.480	1.493	1.472
S_{20}-C_{21}	1.790	1.786	1.805		C_{43}-O_{51}	1.223	1.218	1.230
C_{22}-C_{23}	1.396	1.396	1.397		C_{49}-O_{52}	1.223	1.222	1.235
C_{23}-N_{24}	1.387	1.395	1.388					
N_{24}-C_{25}	1.452	1.459	1.455					
N_{24}-C_{26}	1.379	1.377	1.380					
C_{26}-C_{27}	1.414	1.422	1.405					
C_{27}-C_{16}	1.379	1.397	1.390					
C_{13}-C_{28}	1.462	1.442	1.450					
C_{28}-S_{29}	1.774	1.783	1.789					
S_{29}-C_{30}	1.726	1.733	1.741					

Figure S14. Optimized geometrical coordinates of DFI at the neutral, cation and anionic states.

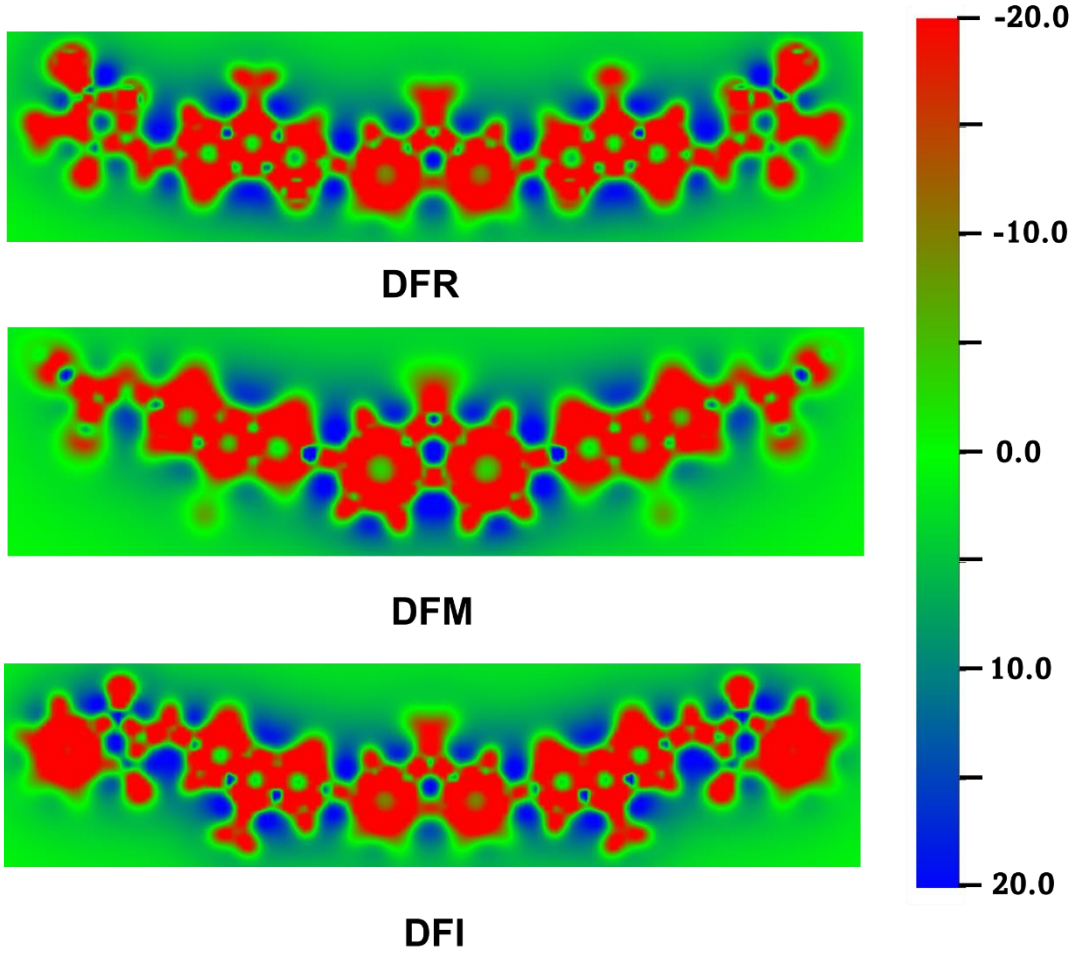

Figure S15. 2D-ICSS Map of the SMEDs showing aromatic and anti-aromatic characteristics.

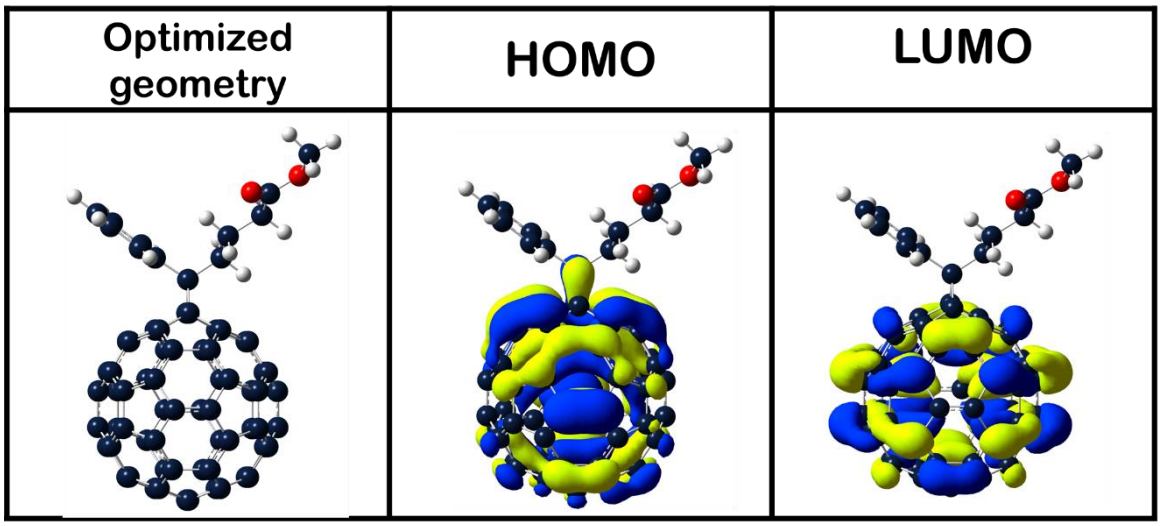

Figure S16. Optimized geometry and computed isosurface of frontier molecular orbitals of $PC_{61}BM$ electron acceptor.

Optimized geometry	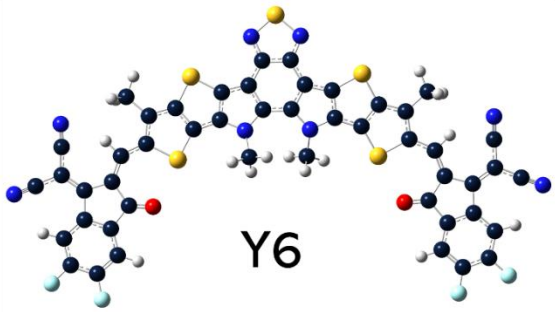
HOMO	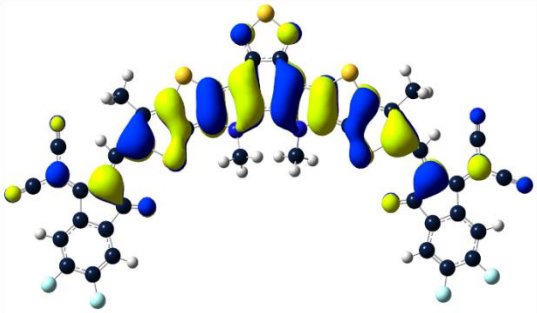
LUMO	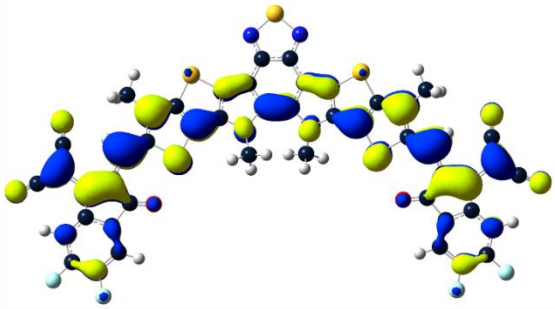
LUMO+1	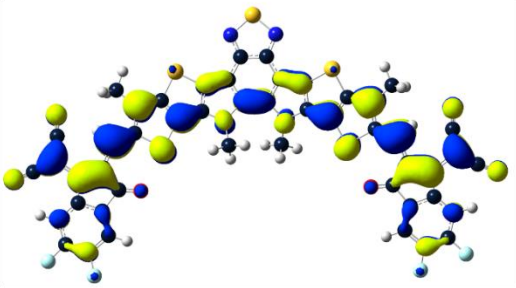

Figure S17. Optimized geometry and computed isosurface plots of the frontier molecular orbitals of Y6 electron acceptor.

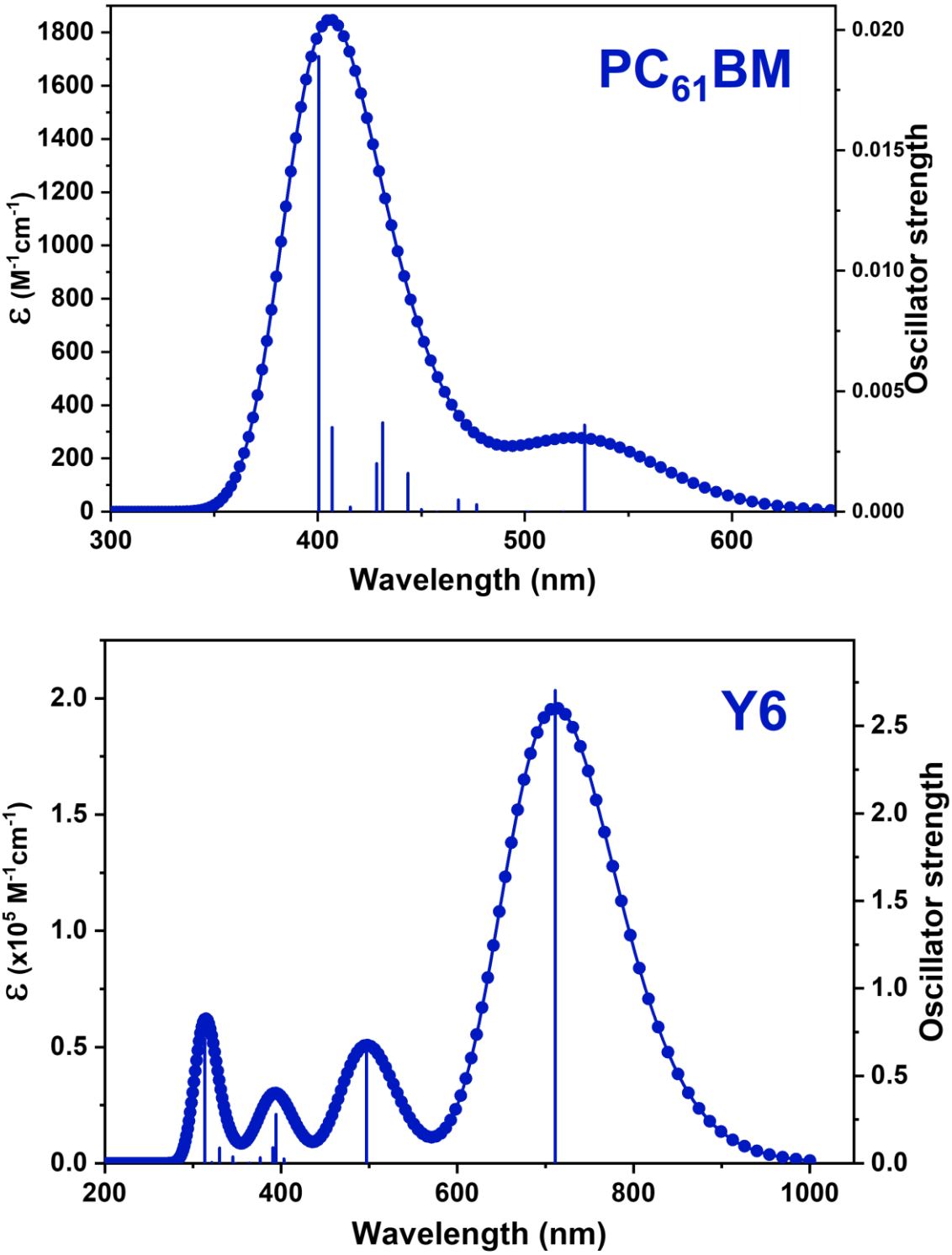

Figure S18. Simulated absorption profiles of $PC_{61}BM$ and Y6 acceptors obtained at the TDDFT/M06-2X/6-311G (d, p)/CPCM($CHCl_3$) level of theory.

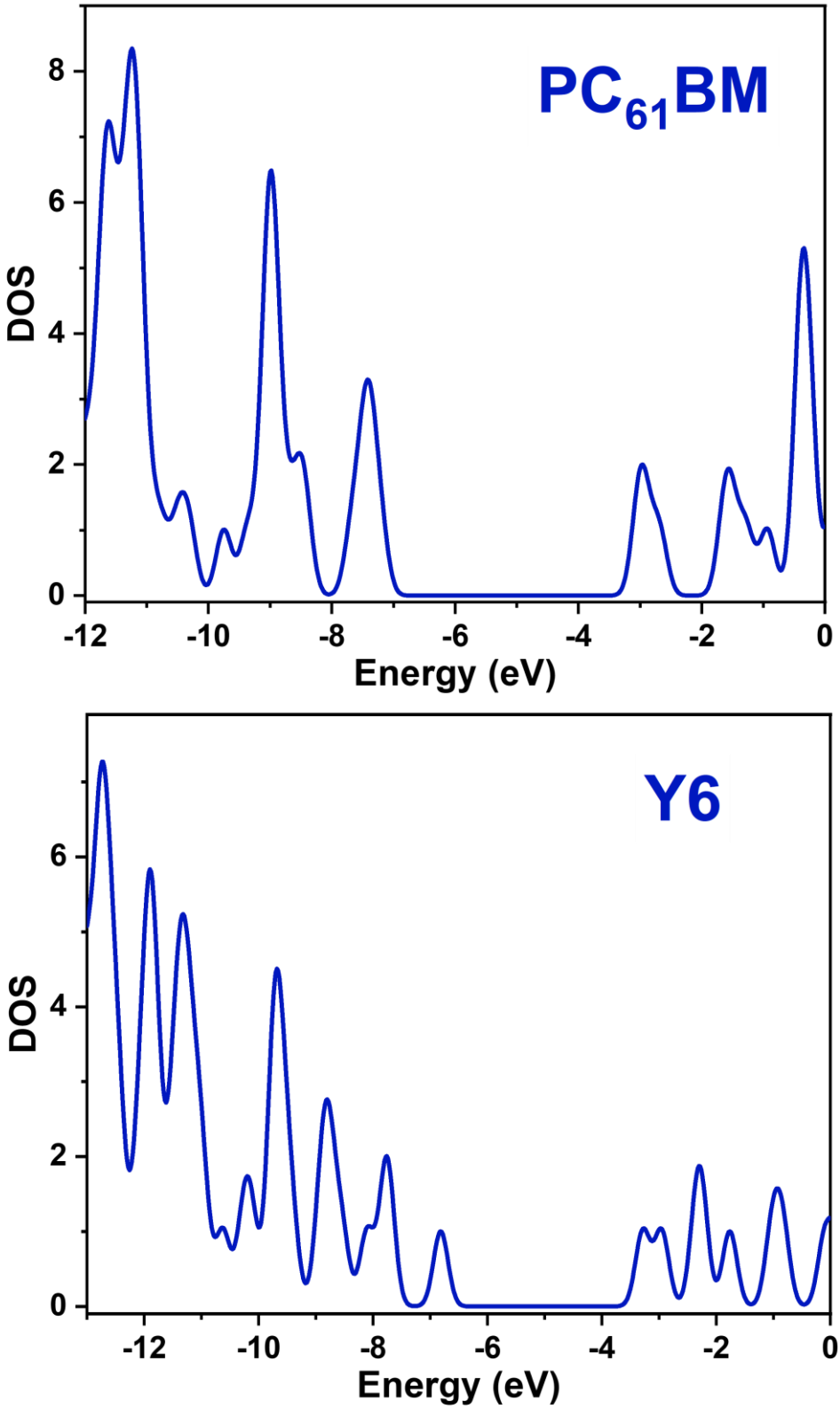

Figure S19. DOS population corresponding to the frontier energy levels of $PC_{61}BM$ and Y6 electron acceptors.

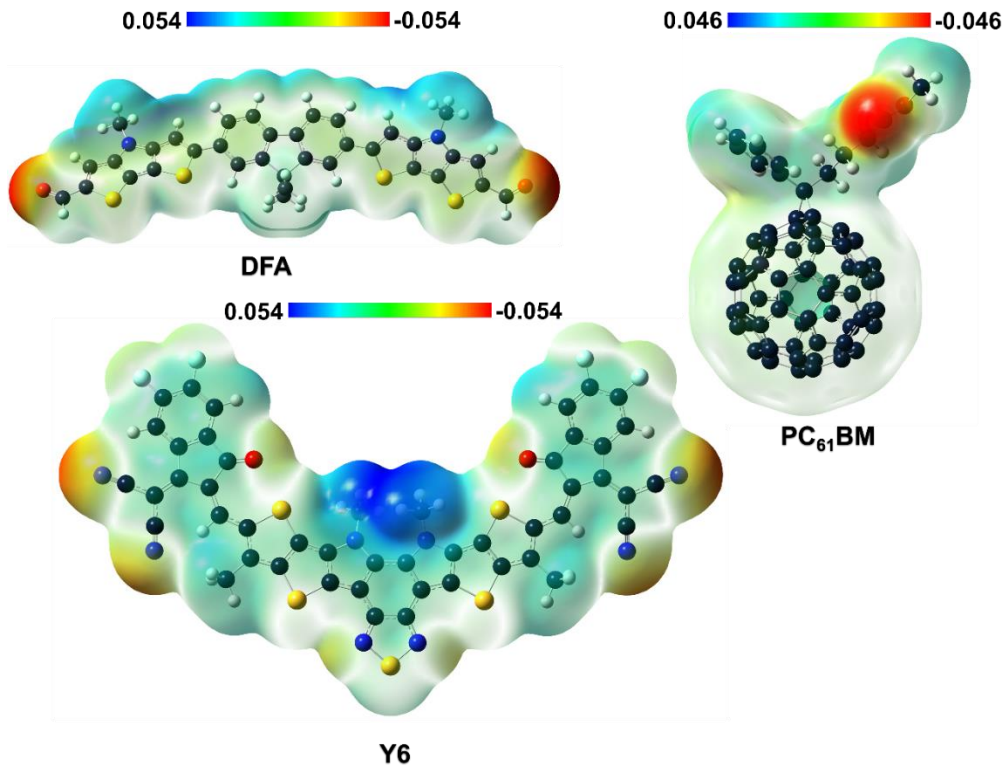

Figure S20. ESP plots of the SMEDs obtained from DFT/B3LYP/6-311G++ (d, p) level of theory.

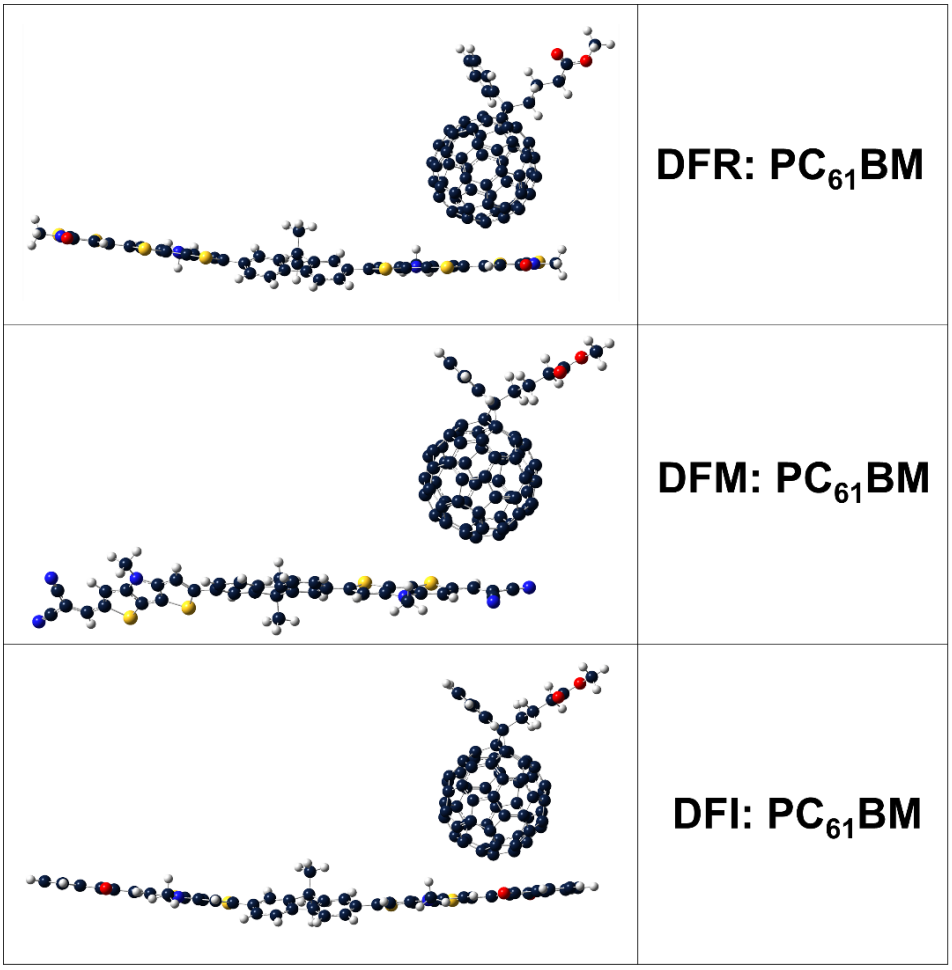

Figure S21. Optimized geometries of SMEDs-$PC_{61}BM$ combination.

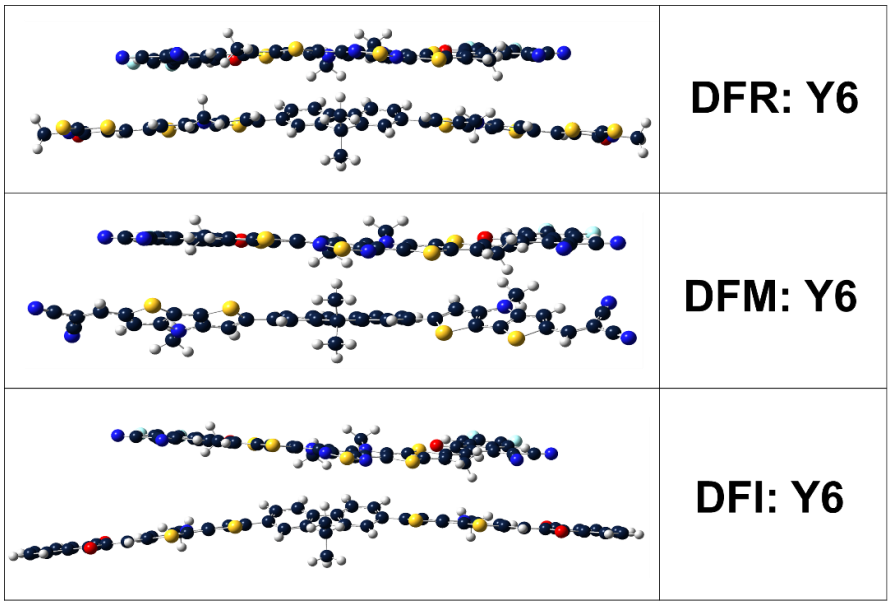

Figure S22. Optimized geometries of SMEDs-Y6 combination.

Tables

Table S1. Computed S_0- S_1 excitation energies with electron volt in parenthesis, oscillator strength (f), major transitions and transient dipole moment of the dyes obtained from B3LYP/6-311G(d, p)/C-PCM(CH_2Cl_2) level of theory.

B3LYP		λ_{max} (nm)	f	Major transitions	μ_e (D)
DFR	S_0-S_1	489.3 (2.534 eV)	4.27	HOMO->LUMO (57%), H-1->L+1 (33%))	3.33
	S_0-S_2	463.8 (2.673 eV)	0.16	H-1->LUMO (44%), HOMO->L+1 (46%)	
DFM	S_0-S_1	476.6 (2.601 eV)	3.82	H-1->L+1 (30%), HOMO->LUMO (63%), H-4->L+2 (2%)	8.44
	S_0-S_2	446.1 (2.779 eV)	0.18	H-1->LUMO (44%), HOMO->L+1 (49%), H-4->L+1 (4%)	
DFI	S_0-S_1	494.3 (2.508 eV)	4.41	H-1->L+1 (32%), HOMO->LUMO (60%), H-4->L+4 (2%)	12.12
	S_0-S_2	464.8 (2.667 eV)	0.16	H-1->LUMO (44%), HOMO->L+1 (47%), H-4->L+1 (4%)	

Table S2. Computed S_0- S_1 excitation energies with electron volt in parenthesis, oscillator strength (f), major transitions and transient dipole moment of the dyes obtained from CAM-B3LYP/6-311G(d, p)/C-PCM(CH_2Cl_2) level of theory.

CAM-B3LYP		λ_{max} (nm)	f	Major transitions	μ_e (D)
DFR	S_0-S_1	538.4 (2.303 eV)	4.37	H-1->L+1 (29%), HOMO->LUMO (64%)	3.69
	S_0-S_2	465.9 (2.661 eV)	0.16	H-1->LUMO (43%), HOMO->L+1 (50%), H-4->L+1 (4%)	
DFM	S_0-S_1	511.6 (2.423 eV)	3.81	H-1->L+1 (27%), HOMO->LUMO (67%), H-4->L+2 (2%)	8.25
	S_0-S_2	445.1 (2.786 eV)	0.18	H-1->LUMO (42%), HOMO->L+1 (52%), H-4->L+1 (3%)	
DFI	S_0-S_1	556.2 (2.229 eV)	4.25	H-1->L+1 (31%), HOMO->LUMO (62%)	11.96
	S_0-S_2	465.1 (2.666 eV)	0.16	H-1->LUMO (44%), HOMO->L+1 (49%), H-4->L+1 (3%)	

Table S3. Computed S_0- S_1 excitation energies with electron volt in parenthesis, oscillator strength (f), major transitions and transient dipole moment of the dyes obtained from M06-2X/6-311G(d, p)/C-PCM(CH_2Cl_2) level of theory.

M06-2X		λ_{max} (nm)	f	Major transitions	μ_e (D)
DFR	S_0-S_1	555.5 (2.232 eV)	3.26	HOMO->LUMO (95%), H-1->L+1 (3%)	3.13
	S_0-S_4	491.2 (2.524 eV)	0.71	H-1->L+1 (95%), HOMO->LUMO (4%)	
DFM	S_0-S_1	537.0 (2.309 eV)	3.34	HOMO->LUMO (97%)	8.86
	S_0-S_4	446.4 (2.777 eV)	0.66	H-3->L+1 (25%), H-2->LUMO (49%), H-1->L+1 (25%)	
DFI	S_0-S_1	579.6 (2.534 eV)	3.47	HOMO->LUMO (96%), H-1->L+1 (3%)	12.5
	S_0-S_4	475.8 (2.534 eV)	0.71	H-1->L+1 (93%), HOMO->LUMO (3%)	

Table S4. Computed S0- S1 excitation energies with electron volt in parenthesis, oscillator strength (f), major transitions and transient dipole moment of SMEDs-$PC_{61}BM$ acceptor combination obtained from M06-2X/6-311G(d, p)/C-PCM(CH_2Cl_2) level of theory.

M06-2X		λ_{max} (nm)	f	Major transitions	μ_e (D)
DFR-$PC_{61}BM$	S_0-S_2	509.4 (2.434 eV)	0.14	H-2->LUMO (91%), H-7->L+1 (3%)	7.14
	S_0-S_4	506.1 (2.450 eV)	1.22	H-3->LUMO (16%), HOMO->LUMO (11%), HOMO->L+1 (13%), HOMO->L+3 (17%), H-2->L+1 (8%), H-1->LUMO (7%), H-1->L+1 (7%), H-1->L+4 (8%)	
DFM-$PC_{61}BM$	S_0-S_5	480.8 (2.579 eV)	3.63	H-2->LUMO (92%), H-5->L+1 (3%)	10.33
	S_0-S_8	449.9 (2.756 eV)	0.19	H-1->L+4 (26%), HOMO->L+3 (62%), H-9->L+8 (2%), HOMO->L+2 (5%)	
DFI-$PC_{61}BM$	S_0-S_1	525.6 (2.359 eV)	0.58	H-2->LUMO (55%), H-3->LUMO (3%), H-1->LUMO (5%), HOMO->LUMO (5%), HOMO->L+1 (5%), HOMO->L+3 (6%)	12.3
	S_0-S_4	517.2 (2.397 eV)	1.63	H-2->LUMO (30%), H-2->L+1 (10%), HOMO->L+3 (23%) H-1->L+1 (5%), H-1->L+4 (8%), HOMO->L+1 (9%)	

Table S5. Computed S0- S1 excitation energies with electron volt in parenthesis, oscillator strength (f), major transitions and transient dipole moment of SMEDs-Y6 acceptor combination obtained from M06-2X/6-311G(d, p)/C-PCM(CH_2Cl_2) level of theory.

M06-2X		λ_{max} (nm)	f	Major transitions	μ_e (D)
DFR-Y6	S_0-S_1	608.8 (2.037 eV)	2.38	H-1->LUMO (83%), H-6->L+1 (7%), H-5->L+1 (2%), H-1->L+4 (2%)	7.95
	S_0-S_5	486.9 (2.546 eV)	4.15	H-2->L+3 (29%), HOMO->L+2 (61%), H-7->L+7 (2%)	
DFM-Y6	S_0-S_1	606.2 (2.045 eV)	2.31	H-1->LUMO (84%), H-6->L+1 (7%)	8.87
	S_0-S_5	493.8 (2.511 eV)	4.48	H-2->L+3 (29%), HOMO->L+2 (64%) H-7->L+9 (2%)	
DFI-Y6	S_0-S_1	611.8 (2.027 eV)	2.26	H-1->LUMO (71%), HOMO->LUMO (14%), H-6->L+1 (4%), H-3->L+1 (5%)	12.98
	S_0-S_5	473.9 (2.616 eV)	3.70	H-2->L+3 (26%), HOMO->L+2 (57%), H-1->L+2 (7%)	

Table S6. Computed bond length alternation and energy levels of the SMEDs at the cation and anionic states

	BLA_{neu}[a] (Å)	BLA_{cat}[b] (Å)	BLA_{ani}[c] (Å)	$BLA_{N\rightarrow C}$[d] (Å)	$BLA_{N\rightarrow A}$[e] (Å)	$HOMO_{cat}$[f] (eV)	$LUMO_{cat}$[f] (eV)	H-L_{cat}[f] (eV)	$HOMO_{ani}$[g] (eV)	$LUMO_{ani}$[g] (eV)	H-L_{ani}[g] (eV)
DFR	-0.161	-0.061	-0.082	-0.154	-0.03	-8.52	-4.48	4.04	-4.08	-1.90	2.18
DFM	-0.357	-0.037	-0.005	-0.173	-0.072	-9.02	-4.94	4.08	-4.48	-2.10	2.38
DFI	-0.126	-0.042	-0.004	-0.202	-0.141	-8.54	-4.48	4.06	-4.28	-1.92	2.36

[a,b,c]-variation of bond length alternation of the SMEDs at the neutral, oxidized and reduced state respectively; [d, e]-variation of BLA transformation from neutral to oxidized/reduced charged states respectively; [f, g]- frontier energy levels at the oxidized and reduced states respectively.

Table S7. Interaction energy of the SMEDs upon combination with the electron acceptors $PC_{61}BM$ and Y6.

D-A	Interaction energy (kcal/mol)	D-A	Interaction energy (kcal/mol)
DFR-$PC_{61}BM$	-169.70	DFR-Y6	-166.29
DFM-$PC_{61}BM$	-156.37	DFM-Y6	-142.76
DFI-$PC_{61}BM$	-169.92	DFI-Y6	-153.20